Journal of Marine Research, 72, 165–181, 2014

The transport of nutrient-rich Indian Ocean water through the Red Sea and into coastal reef systems

by James H. Churchill[1,2], Amy S. Bower[1], Daniel C. McCorkle[3], and Yasser Abualnaja[4]

ABSTRACT

Driven by upwelling-favorable monsoon winds, nutrient-rich Gulf of Aden Intermediate Water (GAIW) enters the Red Sea from the Indian Ocean each summer. Hydrographic and velocity data acquired in autumn 2011 provide the first indication that GAIW is carried rapidly northward along the eastern Red Sea margin in a well-defined subsurface current with speeds >30 cm s^{-1}. The nutrient-rich (NO_2 + NO_3 concentrations up to 17 μmol l^{-1}) GAIW overlaps the euphotic zone and appears to fuel enhanced productivity over depths of 35–67 m. GAIW is broadly distributed through the Red Sea, extending northward along the eastern Red Sea boundary to $\sim$24°N and carried across the Red Sea in the circulation of a basin-scale eddy. Of particular significance is the observed incursion of GAIW into coastal areas with dense coral formations, suggesting that GAIW could be an important source of new nutrients to coral reef ecosystems of the Red Sea.

1. Introduction

The Red Sea is a nearly completely enclosed basin, with the sole significant connection to the open ocean through the narrow ($\sim$25-km width), shallow ($\sim$160-m sill depth) Bab al Mandeb (BAM) Strait at its southern end (Fig. 1). Heileman and Mistafa (2008) have classified the Red Sea as a Class 1, highly productive, large marine ecosystem. The introduction of new water-borne nutrients to the Red Sea is limited to a single principal source, a seasonal intrusion of Indian Ocean water (Khimitsa and Bibik, 1979; Souvermezoglou et al., 1989) known as Gulf of Aden Intermediate Water (GAIW), which flows through BAM during summer (June–September). This seasonal influx results from upwelling-favorable monsoon winds over the western Gulf of Aden, which elevate GAIW above the BAM sill depth and produce a hydrostatic pressure gradient driving GAIW northward through the strait (Patzert, 1974). Typically sandwiched between outward flowing layers of Red Sea Surface Water above and Red Sea Overflow Water below, GAIW streams through BAM

1. Department of Physical Oceanography, Woods Hole Oceanographic Institution, Woods Hole, MA 02543.
2. Corresponding author ***e-mail: jchurchill@whoi.edu***
3. Department of Geology and Geophysics, Woods Hole Oceanographic Institution, Woods Hole, MA 02543.
4. Red Sea Research Center, King Abdullah University of Science and Technology, Thule, Saudi Arabia.

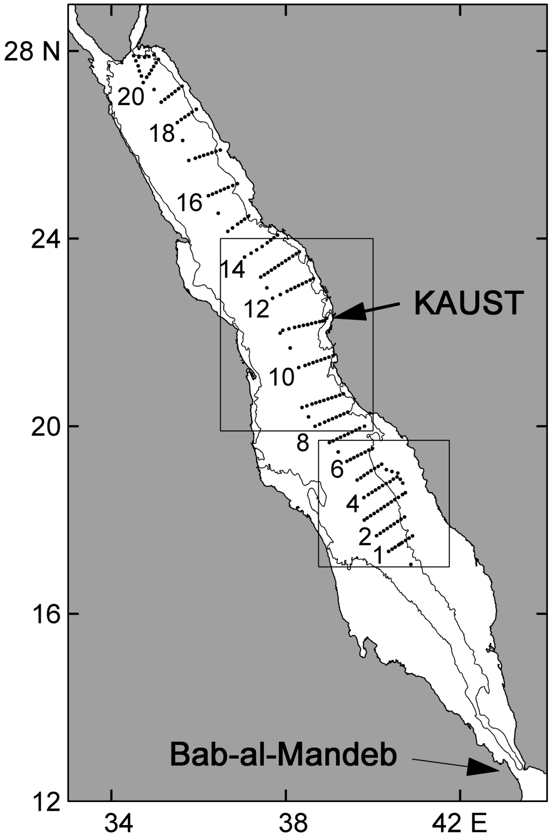

Figure 1. CTD stations of the September-October 2011 *R/V Aegaeo* cruise in the Red Sea, with transect numbers (1–20) indicated. The contour lines roughly mark the 150-m isobath at the upper edge of the Red Sea's central basin. As shown in subsequent figures, the coastal region inshore of the basin is complicated and includes many channels of >150-m depth, which are not contoured above.

over a 30- to 120-m depth range (Palzert, 1974; Murray and Johns, 1997) and at a rate of 0.22–0.36 Sv (Maillard and Soliman, 1986; Murray and Johns, 1997; Sofianos et al., 2002) It enters the Red Sea as a relatively cold (17.4°C at 75 m in BAM vs 31.4°C in the top 10 m), fresh (35.8 vs 37.4 psu) and nutrient-rich (e.g., NO_3, 23.5 vs 0.9 μmol l^{-1}) water mass (Poisson et al., 1984; Maillard and Soliman, 1986; Souvermezoglou et al., 1989).

Observations of GAIW propagation through the Red Sea have thus far been limited principally to temperature and Conductivity-Temperature-Depth (CTD) data. The most-detailed study of a GAIW intrusion to date is that of Sofianos and Johns (2007), who utilized CTD data from an August 2001 cruise of the Red Sea. They found GAIW to be concentrated on the eastern Red Sea margin, with core property anomalies decreasing significantly between BAM and 16°N. The sole study to address the rate at which GAIW moves northward through the Red Sea is that of Smeed (1997). Using temperature profiles collected over 1967–1989, Smeed traced the seasonal northward migration of the GAIW temperature minimum. On the basis of the timing and location of the temperature minimum seen in the full 23-year data set, he estimated that GAIW propagates northward at an average rate of 6 cm s^{-1}. This is considerably slower than the 25- to 50-cm s^{-1} speed at which GAIW flows through BAM (Maillard and Soliman, 1986; Murray and Johns, 1997), which Smeed attributed to lateral spreading of GAIW as it moves northward.

The previous studies have left unresolved a number of critical issues regarding the movement of GAIW through the Red Sea. These include the actual velocity at which GAIW is carried northward from BAM; the manner in which GAIW movement is influenced by the numerous eddies that populate the Red Sea basin (Quadfasel and Baudner, 1993; Sofianos and Johns, 2007; Zhai and Bower, 2013; Zhan et al., 2014); and perhaps most importantly, the extent to which nutrient-rich GAIW enters the coral ecosystems of the coastal Red Sea. Here we address these and other issues related to the movement of GAIW using an extensive data set acquired in autumn 2011. The data include shipboard CTD and Acoustic Doppler Current Profiler (ADCP) data, nutrient measurements from discrete water samples and satellite altimeter-derived sea level anomaly (SLA) fields.

2. Methods

The data presented here were collected from the *R/V Aegaeo* during Leg 1 of the KAUST 2011 Red Sea Expedition (15 September–10 October). Temperature, salinity, dissolved oxygen, fluorescence and Photosynthetically Active Radiation (PAR) profiles were obtained at 206 stations, and along 20 across-basin transects (Fig. 1), using a SeaBird Electronics SBE9+ CTD profiler outfitted with an SBE oxygen sensor, a WETLabs integrated chlorophyll-a/turbidity sensor and a Biospherical underwater PAR light sensor. Water samples for postcruise nutrient analysis and for onboard oxygen sensor calibration were collected in 10-l Niskin bottles. These samples were acquired from stations along each transect at nominal depths of 25, 50, 100, 200, 300, 400, 500, 600 and 1000 m. The nutrient samples were frozen immediately following acquisition. Inorganic nutrients were measured using standard colorimetric methods on a Lachat QuickChem 8000 flow injection analyzer at the Woods Hole Oceanographic Institution Nutrient Facility (Lachat QuickChem Method 31-107-04-1-E [Wood et al., 1967] for $NO_2 + NO_3$; Lachat QuickChem Method 31-115-01-1-H [Murphy and Riley, 1962] for phosphate). Blanks (Milli-Q water) and standards were analyzed routinely within each sample run. Standards were made fresh daily using ACS-certified chemicals and were compared daily to intercalibration performance standards.

The *R/V Aegaeo* was outfitted with a hull-mounted 75-kHz Ocean Surveyor (Teledyne RD Instruments) ADCP. Single-ping measurements, taken over a depth range of about 600 m and at a rate of about 2.5 s per ping, were averaged over 5 min to give vertical profiles of horizontal velocity in 8-m depth bins. The velocities were converted from the

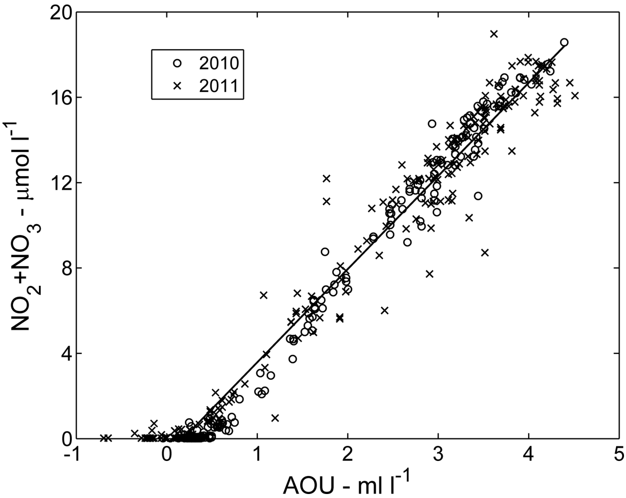

Figure 2. Plot of $NO_2 + NO_3$ concentration (N) against Apparent Oxygen Utilization (AOU) with the linear regression line relating the two variables superimposed. The regression is used to determine fields of N from CTD data.

ship's reference frame into earth coordinates using the ship's heading from the onboard gyro compass and ship's velocity determined using GPS. The velocity vectors shown here at CTD stations, on map-view plots, were averaged over the time-on-station, typically 0.5–2 h.

In order to resolve the $NO_2 + NO_3$ concentration (hereafter N) fields from the CTD data, we derived a mathematical relationship between N and Apparent Oxygen Utilization (AOU), which can be determined from CTD measurements of salinity, temperature and O_2 concentration. The relationship was determined through linear regression using N values derived from bottle samples taken over depths of 31–1800 m (206 samples from our 2011 survey and 184 from a March 2010 survey of the northern Red Sea) and AOU values determined from CTD measurements coincident with the bottle samples. The plot of N against AOU (Fig. 2) shows a strong linear trend that reflects the influence of organic matter decomposition on both N and AOU (e.g., Broecker, 1974; Takahashi et al., 1985). The linear regression line determined from the N against AOU data is of the form $N = 4.37*AOU - 0.79$ ($R^2 = 0.97$), where N and AOU are in units of μmol l^{-1} and ml l^{-1}, respectively. The slope (intercept) of the regressions determined from either the 2010 or the 2011 data alone differs from the slope (intercept) given above by <0.32 (0.76). The 95% confidence interval of the N estimates determined from the regression line (as determined from the residuals from the regression) is roughly $\pm 2\,\mu$mol l^{-1}. Concentrations of PO_4 and SiO_2 also exhibited a linear relationship with AOU, allowing us to derive expressions, using the approach above, for PO_4 and SiO_2 concentrations as a function of AOU. Linear trends of Red Sea nutrient concentrations with AOU have also been reported by Naqvi

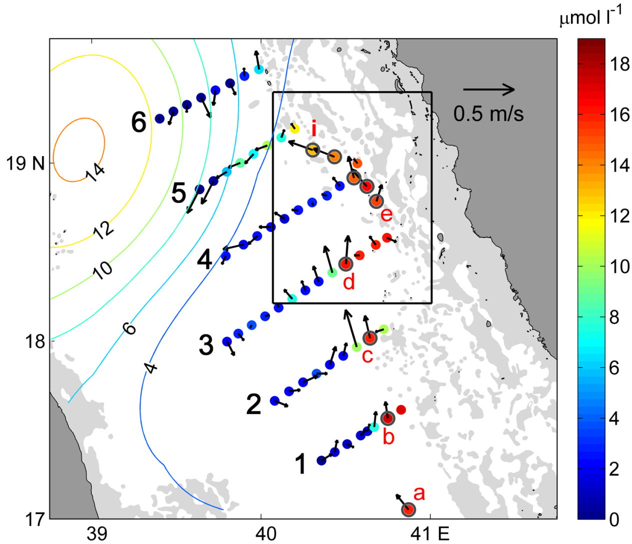

Figure 3. Expanded view of the region enclosed by the southern rectangle in Figure 1, with the 66-m $NO_2 + NO_3$ concentration and mean 66-m velocity (vectors) at each CTD station. Nutrient-rich water appears to be carried in a strong northward current along the eastern margin of the survey region to transect 5 and diverted southwestward along transect 5. The superimposed sea level anomaly (SLA, in cm) field of 21 September 2011 shows a basin-scale eddy with an SLA gradient, which would produce a southwestward flow in the area of transect 5. The lightly colored areas are coral islands and shoals of depth <50 m. Those shallow areas off the eastern shore are part of the Farasan Banks. Circled stations labeled a–i are those at which the high-velocity/nutrient-enriched core of the GAIW intrusion was sampled.

et al. (1986), who analyzed data from a May 1983 cruise that spanned the full length of the Red Sea.

The SLA field shown in Figure 3 was computed with respect to the CLS01 (Centre de Localisation des Satellites) long-term mean sea surface height. The field, obtained from AVISO (http://www.aviso.oceanobs.com/), combines the data of all available satellites in an objectively mapped grid of SLA with 0.25° grid spacing. SLA, rather than absolute dynamic topography, was utilized in our study because the mean dynamic topography is not available for the Red Sea. This is because of a lack of *in situ* hydrographic and velocity data, which AVISO uses to generate maps of absolute dynamic topography in other areas. Recently, SLA has been employed as an integral part of studies of Red Sea dynamics by Zhai and Bower (2013) and Zhan et al. (2014).

3. Results

Our observations reveal three distinct GAIW features: 1) a northward-moving stream of nutrient-rich GAIW extending to ~19°N, 2) a filament of GAIW carried across the Red Sea

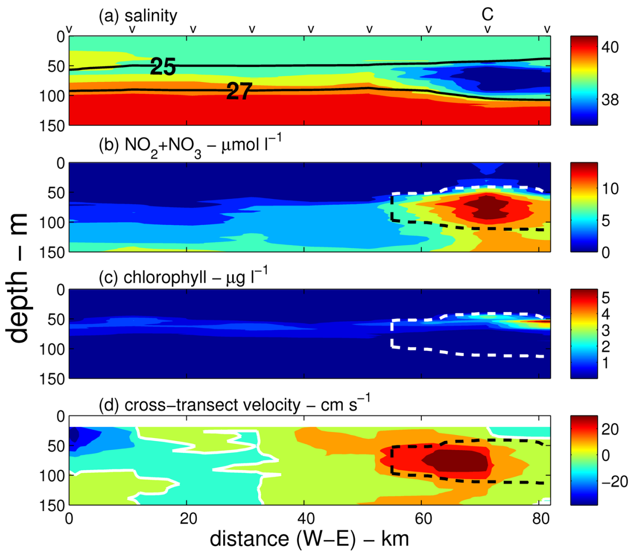

Figure 4. Water properties along transect 2 (Fig. 3) The solid black contours on the salinity field (a) mark the 25 and 27 σ_t surfaces. The dotted line curves on the other sections (b–d) outline the GAIW water intrusion, which encompasses subsurface maxima of $NO_2 + NO_3$ (b), chlorophyll concentration (c) and northward (across-transect) velocity (d). The white lines in (d) are zero velocity contours. Also shown is station c of the along-GAIW section of Figure 3.

basin in the circulation of an anticyclonic eddy, and 3) highly dilute but identifiable GAIW appearing north of 19°N. These features are dealt with separately below. Feature 1 is most intensively analyzed, as its boundaries and properties are best resolved by the salinity and nutrient fields.

a. The GAIW stream to 19°N

The 66-m N field, computed from the CTD measurements as described above, show GAIW with high N (reaching 17 μmol l^{-1}) extending from the survey's southernmost station (at 17°N) to 19°N (Fig. 3). Concentrations of PO_4 and SiO_2 (as estimated from the CTD measurements) show a similar pattern. Superimposing 66-m velocities, measured by the *R/V Aegaeo*'s ADCP, over the N field (Fig. 3) reveals what appears to be a continuous stream of high-N GAIW flowing northward to transect 5 (19°N). The GAIW in this stream is distinguished by high N (>14 μmol l^{-1}) and low salinity (37.5 vs. 38.5 psu above). It spans a depth range of ~35–120 m and a σ_t range of ~25–27.5 (e.g., Figs. 4 and 5).

Our measurements provide the first indication that the GAIW intrusion is transported northward through the southern Red Sea in a well-defined subsurface current. This current is clearly visible in the fields of across-transect (roughly to the NNW) velocity measured along transects 1–4. It appears in the velocity field of transect 2, for example, as a 15- to

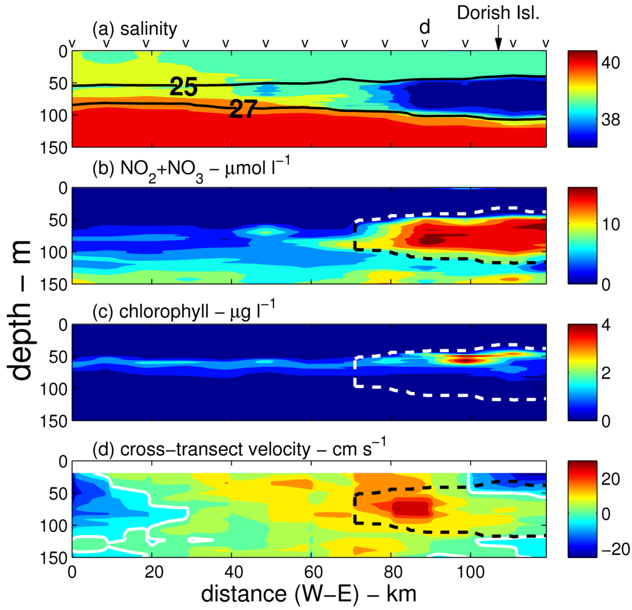

Figure 5. The same as Figure 4 except showing water properties along transect 3. The arrow above (a) marks the location of Dorish Island, which is at the outer boundary of the area of isolated coral shoals and islands penetrated by transects 1–3 (see Fig. 6). Also indicated is station d of the along-GAIW section of Figures 3 and 6.

40-cm s^{-1} flow extending over ~35–115 m and roughly coinciding with the high-N core of the GAIW intrusion (Fig. 4). The across-transect velocity field of transect 3 also shows a strong (15–30 cm s^{-1}) NNW-ward current coinciding with the high-N core of the GAIW intrusion (Fig. 5). However, this current does not encompass the major fraction of the GAIW measured along the transect. Roughly 60% of the GAIW signature is situated shoreward of the high-velocity (15–30 cm s^{-1}) core of the current and is predominately within a 0- to 10-cm s^{-1} NNW-ward flow (Fig. 5). As detailed further below, we hypothesize that this weakly flowing GAIW may have emerged from the reef area directly upstream (to the SSE) of transect 3 (Fig. 3).

Our measurements are also the first to show nutrient-rich GAIW in proximity to Red Sea coral islands and reefs. This is apparent over transects 1–3, which extend eastward from the Red Sea basin through an area of isolated coral shoals and islands, and terminate within a few kilometers of a near-shore region of dense coral formations (part of Farasan Banks) (Fig. 3). Vertical sections of salinity and N along these transects (e.g., Figs. 4 and 5) show the high-N GAIW intrusion confined to the eastern end of each transect, and extending into the area of isolated coral islands and reefs. Notably, the GAIW observed along transect 3 encompasses an offshore coral feature known as Dorish Island (Figs. 5 and 6). The frictional

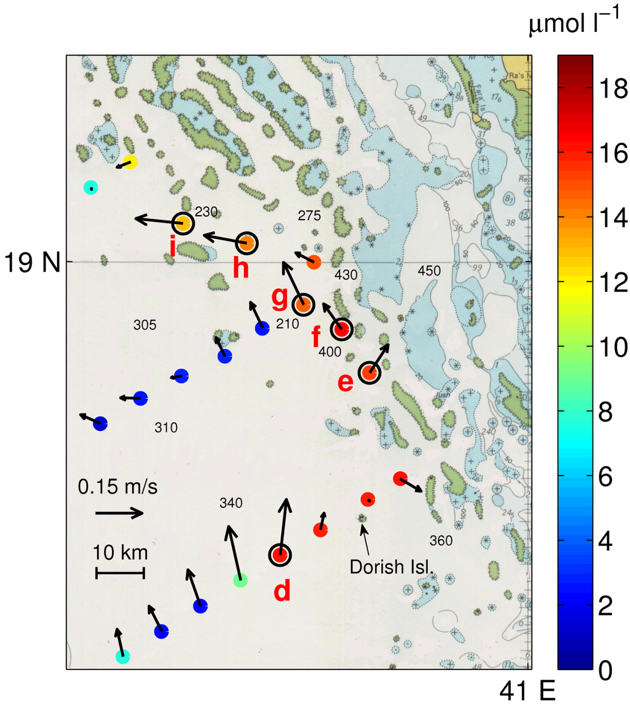

Figure 6. $NO_2 + NO_3$ concentration at 66 m and vertically averaged velocity (over 35–120 m) at each CTD station superimposed on a bathymetric chart (United Kingdom Hydrographic Office) of the area outlined by the box in Figure 3. The circled stations labeled d–i are those at which the high-velocity core of the GAIW intrusion was sampled (see also Fig. 3). Chart depths, shown at selected locations, are in meters. Islands are shaded green, and bottom depths <20 m are shaded light blue.

influence of the near-shore coral features may account for the relatively weak flow of the GAIW observed at the eastern end of transects 1–3 (Figs. 3–6).

Penetration of GAIW into the region of dense coral formations is observed at transect 4, which extends eastward from the Red Sea basin into a deep (>150 m) channel fringed by coral islands. GAIW observed along this transect is largely contained within the channel (Figs. 3 and 6). Data taken at four other stations within the channel (circled in Figs. 3 and 6) show a stream of GAIW occupying roughly the same depth and density range as the GAIW seen along transects 1–3 (Fig. 7). The depth-averaged GAIW flow at the northernmost stations within the channel is directed to the northwest, roughly along the channel axis. Notably, the depth-averaged GAIW flow at the southernmost channel station (station e in Fig. 6) is to the northeast, further into the near-shore coral island and shoal region. The apparent continuity of the jet carrying GAIW across transects 1–3 and through the channel at transect 4, together with the absence of GAIW at transect 4 stations offshore of the

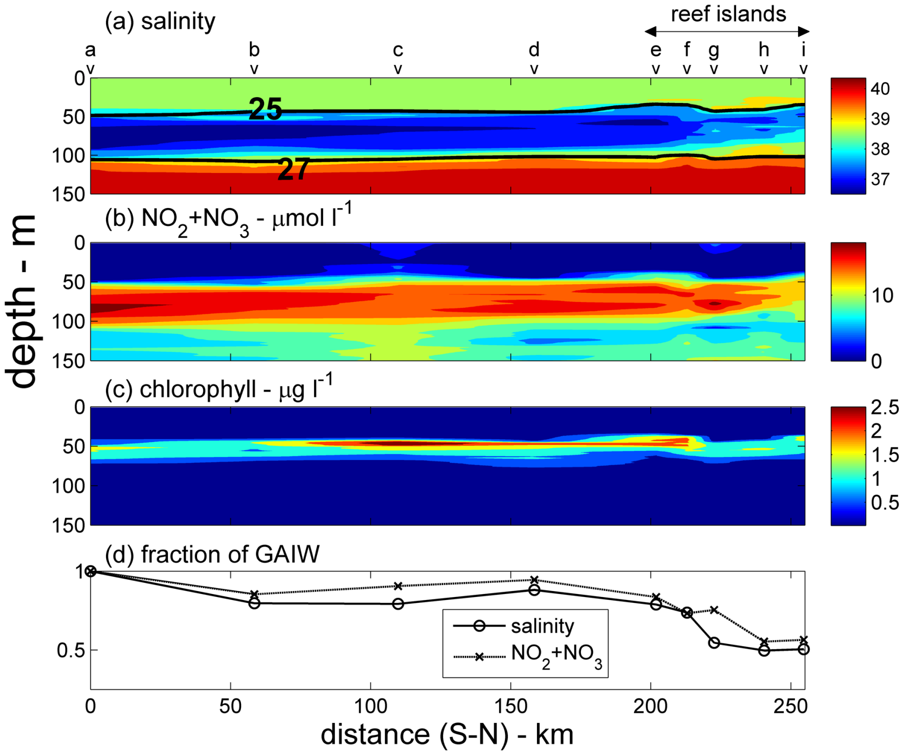

Figure 7. Properties of the high-velocity/nutrient-enriched GAIW stream sampled in the basin and in the coral island channel. Property fields (a–c) are derived using data from the circled stations (labeled a–i) in Figures 3 and 6. Estimated “GAIW fraction” of salinity and NO_2+ NO_3 within the density band (27.25 $>=$ σ_t $>=$ 24.7) occupied by the GAIW intrusion is shown in (d).

channel (Figs. 3 and 6), indicates that the nutrient-rich GAIW intrusion had very likely been diverted into the coral island–fringed channels north of transect 3. Furthermore, it is possible that GAIW had extended, unobserved, into the deeper channels ($>$120 m) of the coral island and shoal area just shoreward of transects 1–3.

To quantify the GAIW volume and N transport across transects 1–4, we interpolated measurements of N and across-transect velocity along each transect onto a standard grid and integrated the velocity, and the product of velocity and N, over the cross section of GAIW. To outline this cross section, we specified the boundaries of the GAIW in the vertical profiles of the interpolated salinity fields using criteria developed through examination of CTD-derived salinity and nutrient profiles. The criteria are that the GAIW is present in profiles in which the minimum salinity over the 65- to 85-m depth range is $<$38.7 practical salinity units (psu) and that the GAIW layer extends between salinity bounds of S_T at the top and S_B at the base (Figs. 4 and 5). The results shown here (Figs. 4 and 5; Table 1) were

Table 1. Cross-transect (positive to the northwest) fluxes of volume and $NO_2 + NO_3$ (N) contained within the Gulf of Aden Intermediate Water intrusion observed along transects 1–4. As detailed in the text, the uncertainty levels (in brackets) account for the sensitivity of the flux to the choice of upper and lower salinity limits vertically bounding the GAIW.

Transect	Volume flux (Sv)		N flux (mol s^{-1})	
1	0.19	$[-0.01 + 0.01]$	2.5×10^3	$[-0.1 + 0.1] \times 10^3$
2	0.34	$[-0.04 + 0.05]$	3.6×10^3	$[-0.3 + 0.4] \times 10^3$
3	0.36	$[-0.05 + 0.04]$	4.4×10^3	$[-0.3 + 0.3] \times 10^3$
4	0.12	$[-0.03 + 0.02]$	1.2×10^3	$[-0.1 + 0.1] \times 10^3$

computed using $S_T = 38.65$ and $S_B = 39.8$ psu. To assess the sensitivity of the computed fluxes to the choice of GAIW salinity bounds, fluxes were also computed using bounds, deemed reasonable from examination of the salinity and N profiles, that gave the minimum and maximum vertical GAIW range ($S_T = 38.4$, $S_B = 39.4$; and $S_T = 38.65$, $S_B = 40.2$ psu, respectively). The results were used to assign uncertainty intervals to the computed fluxes (Table 1), which were no more than 15% of the values computed with $S_T = 38.65$ and $S_B = 39.8$ psu.

Magnitudes of the N-fluxes across transects 1–3 (Table 1) are comparable to the estimates of 3.9–4.5 $\times$ 10^3 mol s^{-1} for GAIW N-flux through BAM (Souvermezoglou et al., 1989). Both the net volume-flux and N-flux increase considerably, by roughly a factor of 1.8, going from transect 1 to 3. This may reflect high-frequency, locally wind-driven, fluctuations in GAIW inflow through BAM (Murray and Johns, 1997). This flux increase may also be partly due to the transport across transects 2 and 3 of GAIW that had flowed unobserved through the coral island and shoal region shoreward of the upstream (more southern) transects. In particular, the easternmost 20 km of transect 3 extends into an indentation of the basin, directly northwest of a coral island and shoal area (Figs. 3 and 6). The N-flux of GAIW across this portion of the transect is 0.8×10^3 mol s^{-1} and roughly equals the increase of GAIW N-flux from transects 2 to 3 (Table 1). GAIW volume-fluxes and N-fluxes across transect 4 are considerably smaller ($<\frac{1}{2}$) than the fluxes measured across transects 1–3, probably because of unobserved GAIW flow in the coral channel region onshore of transect 4 (Figs. 3 and 6).

To determine the extent to which the high nutrient concentrations of GAIW overlap the euphotic zone, we calculated a representative PAR profile by averaging all mid-day (9:00–15:00 local time) PAR profiles taken along transects 1–3. The averaged PAR declines to 12.7% of its 2-m value by 35 m (roughly at the top of the GAIW intrusion), and further decreases to 1% of its 2-m value by 67 m. Along transects 1–3, chlorophyll concentrations, determined from CTD-fluorometer data, tend to be largest within this 35- to 67-m depth band of high-N GAIW and available PAR (Figs. 4c and 5c), consistently exceeding the maximum concentration in the basin water farther offshore (Fig. 8). This tendency for chlorophyll concentrations to be relatively high in GAIW suggests that the combination

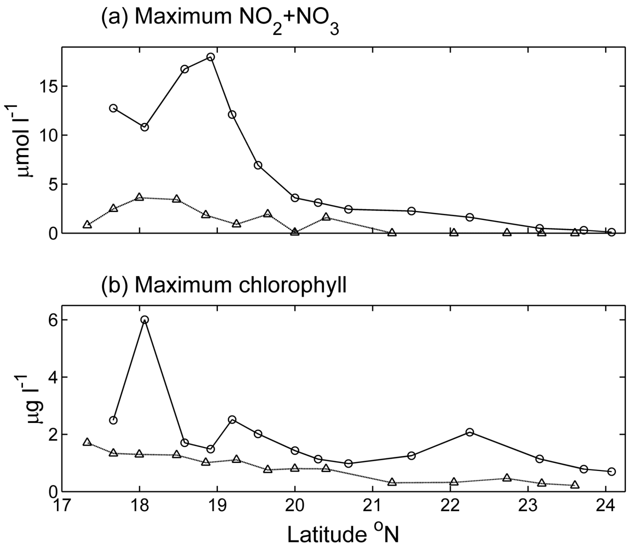

Figure 8. As a function of latitude, maximum $NO_2 + NO_3$ (a) and chlorophyll concentration (b) in the 10- to 75-m depth range at the easternmost (circles/solid line) and westernmost (triangles/dashed line) stations of transects 1–14.

of available PAR and high nutrient concentrations may have fueled enhanced productivity within GAIW.

Previous observations of GAIW in the southern Red Sea suggest that the intrusion is significantly eroded by vertical mixing (Sofianos and Johns, 2007). To estimate the extent to which the GAIW intrusion streaming through the southern basin and the coral island channel had been altered through mixing and nutrient uptake by primary production, we estimated the proportion of GAIW, relative to that contained in the intrusion at the southernmost (reference) station, by assuming that the GAIW was confined to a distinct density band ($\sigma_t = 24.7 - 27.25$) and mixed equally with the water above and below. The GAIW fraction at a station, n, was estimated from salinity (S) by $f_S(n) = (S_n - S_a)/(S_0 - S_a)$, where S_n and S_0 are, respectively, the mean salinities within the specified GAIW density band at n and at the reference station, and S_a is the mean of the salinities just above and below the GAIW layer. A similar expression was used to estimate the GAIW fraction based on N (f_N). Here (Fig. 7d) we show GAIW fractions at stations in the core of the GAIW stream along transects 1–3 and in the coral island and shoal region penetrated by transect 4 (Figs. 3–6). Both f_N and f_S show no systematic decline going from transect 1 to 3, suggesting relatively weak mixing of the GAIW core with surrounding basin water. In contrast, f_S and f_N decline significantly within the coral island region, suggesting that the GAIW within this region is subjected to more vigorous mixing than in the basin. Such mixing may be important in exposing corals above the ~35-m depth ceiling of the GAIW intrusion to elevated nutrient concentrations.

A significant reduction in N due to primary production would be reflected by a sharper decline in f_N relative to f_S. However, this is not observed in our data; f_N and f_S are comparable in both the basin and the coral island region. The observed downstream decline in GAIW N thus appears to be primarily the result of mixing, with uptake through primary production within the GAIW stream playing a secondary role.

b. GAIW-eddy interaction

The GAIW stream appears to bifurcate at transect 5 with one branch deflected to the southwest, along transect 5, and a second continuing northward, as seen at the easternmost station of transect 6 (Fig. 3). The southwestward flow of GAIW observed along transect 5 on 21 September is consistent with the SLA field of that date (Fig. 3), which reveals a basin-scale anticyclonic eddy encompassing transect 5. The eddy is associated with a local SLA high centered near 19°N, 38°53' E, and an SLA gradient that would produce southwestward flow across transect 5 (Fig. 3). The eddy's circulation inferred from the SLA field is consistent with the near-surface ADCP-derived velocities. In particular, the ADCP-derived velocities acquired at 26-m depth in the region of the eddy (18.4–19.9° N; 39–39.85° E) and during the period 20–23 September 2011 are correlated (through complex correlation analysis; Kundu, 1976) with the geostrophic velocities computed from the SLA field (at the same locations of the ADCP measurements) at an R^2 of 0.7, which is significantly different from 0 at the 95 % confidence level.

On the basis of the ADCP-derived velocities and the circulation inferred by the SLA field, it appears that much of the GAIW stream flowing northward to transect 5 (19° N) is entrained in the eddy's circulation and diverted to the southwest. The mean across-basin (at 237° T) flow of the GAIW entrained in the eddy, determined by averaging ADCP-derived velocities measured along transect 5 within the 25–27.5 σ_t range (which encompasses the GAIW), is 14.3 cm s^{-1}. At this rate, a GAIW parcel would traverse the Red Sea basin in roughly 13 d. As the eddy's SLA signature extended to the western Red Sea coast (Fig. 3), it is possible that the GAIW was carried to the reef communities of the western Red Sea.

c. GAIW north of 19°N

Extension of GAIW north of 19°N is suggested by well-defined vertical salinity minima appearing over all transects north of transect 5. However, the contrast between these minima and the higher salinity water above is, at order 0.25 psu, considerably smaller than the order 1.5 psu contrast between the GAIW salinity minima and the salinity of the overlying water observed south of 19°N. As stable vertical salinity minima may be produced by surface heating and evaporation, ascribing the salinity minima north of 19°N as evidence of GAIW must be done with caution. In judging the possibility that these minima may be due to GAIW, we have set criteria that they be within the 25- to 27.5-σ_t range of the

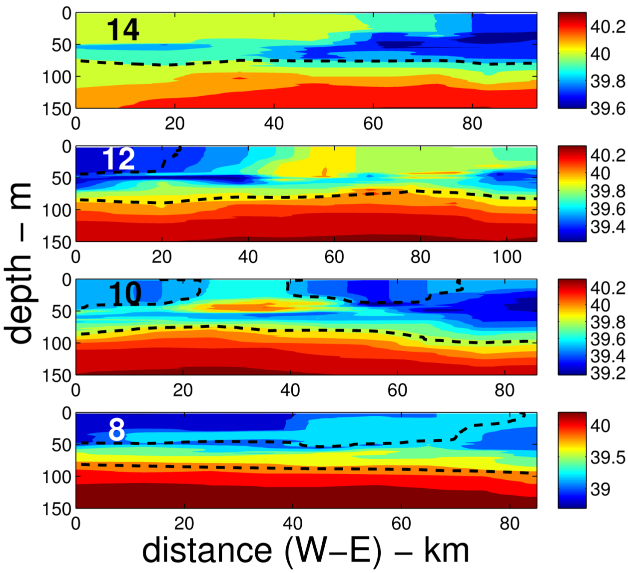

Figure 9. Salinity fields along four transects north of 19°N (Fig. 1). Each field shows the signature of GAIW, in the form of a salinity minimum in the 10- to 100-m depth range, on the eastern boundary of the Red Sea basin. Dashed lines are the 25 and 27 σ_t contours.

GAIW observed south of 19°N and that the lower-salinity water in which they are embedded contain nutrient concentrations larger than those measured in adjacent water of similar depth. Here, we apply these criteria to the salinity minima observed at transects 6–14 (19–24°N). These minima span the full length of a number of these transects. Nevertheless, for all transects, the lowest salinity minimum appears at the easternmost station (Fig. 8). The lower-salinity water associated with these minima roughly spans the 20- to 100-m depth range and is contained within the 25- to 27.5-σ_t density range over which GAIW appears south of 19° N (Fig. 9). The tendency of this lower-salinity water to contain higher N than water of similar depth (and σ_t) within the central basin is evident from the contoured salinity and N fields along each of transects 6–14 (e.g., Fig. 10). Furthermore, both maximum N and average N in the 10- to 75-m depth range are considerably higher at each transect's easternmost station relative to the westernmost station (Fig. 8). The higher N at the eastern margin appears to have enhanced primary productivity relative to the midbasin, as the maximum and average chlorophyll concentration in the 10- to 75-m depth range is also significantly higher on the eastern as compared with the western side of transects 6–14 (Fig. 8). On the basis of these observations, we conclude that the low-salinity water appearing along the eastern boundary at transects 6–14 is GAIW. The salinity minima observed north of transect 14 may also be due to GAIW, but this cannot be reasonably assessed as the low-salinity water in which the minima are embedded has zero, or near-zero, nutrient concentration.

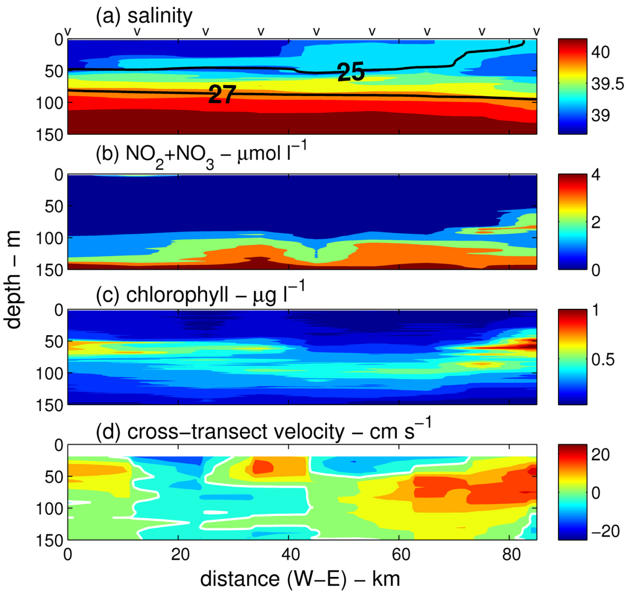

Figure 10. Water property fields along transect 8 (Fig. 1) These fields indicate low-salinity GAIW, roughly confined between the 25 and 27 σ_t surfaces (a). Near the eastern basin margin, the GAIW is carried northward by an order 20 cm s^{-1} current (d) and contains relatively high concentrations of $NO_2 + NO_3$ and chlorophyll (b and c).

The shipboard-ADCP data reveal that the GAIW observed at transects 6–14 is predominately carried northward. The velocities measured in the low-salinity GAIW at the eastern margin of these transects are directed northward, at a rate of 5–25 cm s^{-1} (e.g., Fig. 10), at all but transect 10. This tendency of northward GAIW flow over the central Red Sea is nicely illustrated by the velocity and N fields measured at 66 m (Fig. 11). These show a nearly continuous northward-flowing stream of nutrient-enriched GAIW extending along the eastern Red Sea margin from 19° to 24°N. With the available data, we can only speculate as to why the northward flow of GAIW appears to be interrupted at transect 10. Along-shore velocities measured within the low-salinity, nutrient-enriched water observed at the eastern margin of transect 10 are less than 5 cm s^{-1} in magnitude and predominately directed to the SSE. As transect 10 reaches to within 5 km of the coast, it is unlikely that our measurements missed a near-shore northward flow of GAIW. It is possible that the weak GAIW flow at transect 10 may be partially the result of a temporal weakening of the GAIW inflow through BAM due to local wind forcing (Murray and Johns, 1997). With this exception, the data indicate a northward flow of GAIW along the eastern margin of the Red Sea basin, with high N relative to the central basin water of the same depth, to a latitude of ~24°N.

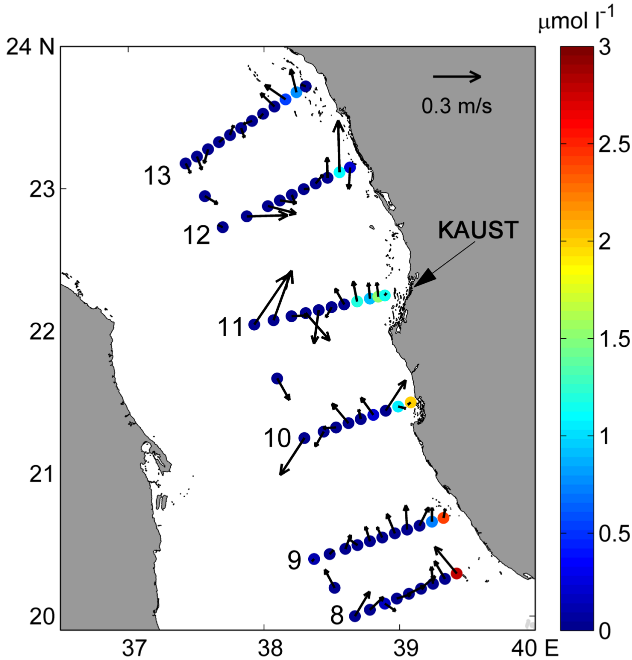

Figure 11. Expanded view of the region enclosed by the northern rectangle in Figure 1, with 66-m $NO_2 + NO_3$ concentration and mean 66-m velocity (vectors) at each CTD station.

4. Summary and discussion

Our analysis of the autumn 2011 cruise data has changed the view of how GAIW propagates through the Red Sea. In a broad sense, the analysis has revealed four modes of GAIW transport.

One is a rapid transit of nutrient-rich GAIW though the southern Red Sea in subsurface flow near the eastern boundary. The speed of this flow, at ~25 cm s^{-1}, is considerably faster than the 6-cm s^{-1} rate of northward GAIW transport previously estimated from temperature data (Smeed, 1997). This strong northward flow and the nutrient-rich GAIW it carries extend to 19°N, >300 km farther north than GAIW had been detected in previous hydrographic observations (Sofianos and Johns, 2007). The magnitude of observed N-transport carried by GAIW between 17 and 19°N is comparable with the N-transport of the GAIW influx through BAM, suggesting that the nutrient flux of GAIW may not be significantly altered by mixing or production as it transits the southern Red Sea.

A second transport mode is cross-basin conveyance of GAIW in the circulation of a basin-scale eddy. Our data show this cross-basin GAIW transport occurring at ~19°N, essentially at the terminus of the rapid northward GAIW flow noted above. This mode of transport may be an important mechanism for rapid movement of GAIW across the Red Sea basin.

Studies by Quadfasel and Baudner (1993) and Sofianos and Johns (2007) have shown that the central Red Sea basin is typically populated with eddies, encompassing velocities of up to 1 m s^{-1}.

A third mode of GAIW transport is observed north of 19°N and takes the form of a stream of dilute GAIW extending along the eastern Red Sea margin to 24°N. Given the prevalence of eddies with the Red Sea basin, which could divert such a flow seaward, it is uncertain whether such a feature may be a common yearly occurrence.

A fourth mode of transport is the incursion of GAIW into coastal reef systems. In our data, this is observed over the outer reefs of the Farasan Banks. More widespread GAIW incursion into Red Sea coral ecosystems is likely. GAIW penetration farther into the Farasan Banks is suggested by the velocities averaged over the GAIW depth range (at site e in Fig. 6), and GAIW may be carried to the coral ecosystems of the eastern Red Sea via the circulation of basin-scale eddies. Furthermore, GAIW-borne nutrients may be delivered to the near-surface reef environment by vertical mixing of GAIW with bordering water masses, as indicated by our measurements over the outer Farasan Banks. As coral health is sensitive to even small variations in nutrients (Marubini and Davies, 1996; Ferrier-Pages et al., 2000; Silverman et al., 2007), the incursion of nutrient-rich GAIW into the coastal areas of the Red Sea could have a profound influence on the resident coral ecosystems. Comprehensive multidisciplinary studies are required to understand how these systems are affected by, and adapt to, nutrient delivery by GAIW.

Acknowledgments. We gratefully acknowledge financial and logistical support for the *R/V Aegaeo* cruise provided by King Abdullah University of Science and Technology (KAUST), and the support of an international group of scientists and technicians during the cruise. We thank in particular S. Swift for work on chart generation during and after the cruise, P. Zhai for her contribution in generating the SLA field, and P. Henderson for nutrient analyses. This research was supported by Award Nos. USA-00002, KSA-00011 and KSA-00011/02 made by KAUST to the Woods Hole Oceanographic Institution.

REFERENCES

Broecker, W. S. 1974. “NO,” a conservative water-mass tracer. Earth Planet. Sci. Lett., *23*, 100–107.

Ferrier-Pages, C., J.-P. Gattuso, S. Dallot and J. Jaubert. 2000. Effect of nutrient enrichment on growth and photosynthesis of the zooxanthellate coral Stylophora pistillata. Coral Reefs, *19*, 103–113.

Heileman, S. and N. Mistafa. 2008. III-6 Red Sea: LME #33, *in* The UNEP Large Marine Ecosystem Report: A Perspective on Changing Conditions in LMEs of the World’s Regional Seas, K. Sherman and G. Hempel, eds. UNEP Regional Seas, Report and Studies No. 182. Nairobi, Kenya: United Nations Environment Programme, 175–186.

Khimitsa, V. A. and V. A. Bibik. 1979. Seasonal exchange in dissolved oxygen and phosphate between the Red Sea and the Gulf of Aden. Oceanol., *9*, 544–546.

Kundu, P. 1976. Ekman veering observed near the ocean bottom. J. Phys. Oceanogr., *6*, 238–242.

Maillard, C. and G. Soliman. 1986. Hydrography of the Red Sea and exchanges with the Indian Ocean in summer. Oceanol. Acta, *9*, 249–269.

Marubini, F. and P. S. Davies. 1996. Nitrate increases zooxanthelae population and reduces skeletogenesis in corals. Mar. Biol., *127*, 319–328.

Murphy, J. and J. P. Riley. 1962. A modified single solution method for determination of phosphate in natural waters. Anal. Chim. Acta, *27*, 31–36.

Murray, S. P. and W. Johns. 1997. Direct observations of seasonal exchange through the Bab el Mandeb Strait. Geophys. Res. Lett., *24*, 2557–2560.

Naqvi, S. W. A., H. P. Hansen and T. W. Kureishy. 1986. Nutrient uptake and regeneration ratios in the Red Sea with reference to the nutrient budgets. Oceanol. Acta, *9*, 271–275.

Patzert, W. C. 1974. Seasonal reversal in the Red Sea circulation, *in* L'oceanographie Physique de la Mer Rouge. Paris: Centre National pour l'Exploitation des Oceans, 55–89.

Poisson, A., S. Morcos, E. Souvermezoglou, A. Papaud and A. Ivanoff. 1984. Some aspects of biogeochemical cycles in the Red Sea with special references to new observations made in summer 1982. Deep-Sea Res., *31*, 707–718.

Quadfasel, D. and H. Baudner. 1993. Gyre-scale circulation cells in the Red Sea. Oceanol. Acta, *16*, 221–229.

Silverman, J., B. Lazar and J. Erez. 2007. Effect of aragonite saturation, temperature, and nutrients on the community calcification rate of a coral reef. J. Geophys. Res., *112*, C05004, doi:10.1029/2006JC003770.

Smeed, D. 1997. Seasonal variation of the flow in the strait of Bab el Mandeb. Oceanol. Acta, *20*, 773–781.

Sofianos, S. S. and W. E. Johns. 2007. Observations of the summer Red Sea circulation. J. Geophys. Res., *112*, C06025, doi:10.1029/2006JC003886.

Sofianos, S. S., W. E. Johns and S. P. Murray. 2002. Heat and freshwater budgets in the Red Sea from direct observations at Bab el Mandeb. Deep Sea Res. II, *49*, 1323–1340.

Souvermezoglou, E., N. Metzl and A. Poisson. 1989. Red Sea budgets of salinity, nutrients, and carbon calculated in the strait of Bab-el-Mandab during the summer and winter season. J. Mar. Res., *47*, 441–456.

Takahashi, T., W. S. Broecker and S. Langer. 1985. Redfield ratio based on chemical data from isopycnal surfaces. J. Geophys. Res., *90*, 6907–6924.

Wood, E., F. Armstrong and F. Richards. 1967. Determination of nitrate in sea water by cadmium copper reduction to nitrite. J. Mar. Biol. Ass. U.K., *47*, 23–31.

Zhai, P. and A. S. Bower. 2013. The response of the Red Sea to a strong wind jet near the Tokar Gap in summer. J. Geophys. Res. Oceans, *118*, 422–434, doi:10.1029/2012JC008444.

Zhan, P., A. C. Subramanian, F. Yao and I. Hoteit. 2014. Eddies in the Red Sea: A statistical and dynamical study. J. Geophys. Res. Oceans, *119*, 3909–3925, doi:10.1002/2013JC009563.

Received: *26 June 2013*; revised: *28 August 2014*.